

---

# Incorporating Prior Knowledge into Neural Networks through an Implicit Composite Kernel

---

**Ziyang Jiang**

Department of Civil and Environmental Engineering  
Duke University  
ziyang.jiang@duke.edu

**Tongshu Zheng**

California Air Resources Board  
tongshu.zheng@arb.ca.gov

**David Carlson**

Department of Civil and Environmental Engineering  
Department of Biostatistics and Bioinformatic  
Duke University  
david.carlson@duke.edu

## Abstract

It is challenging to guide neural network (NN) learning with prior knowledge. In contrast, many known properties, such as spatial smoothness or seasonality, are straightforward to model by choosing an appropriate kernel in a Gaussian process (GP). Many deep learning applications could be enhanced by modeling such known properties. For example, convolutional neural networks (CNNs) are frequently used in remote sensing, which is subject to strong seasonal effects. We propose to blend the strengths of deep learning and the clear modeling capabilities of GPs by using a composite kernel that combines a kernel implicitly defined by a neural network with a second kernel function chosen to model known properties (e.g., seasonality). Then, we approximate the resultant GP by combining a deep network and an efficient mapping based on the Nyström approximation, which we call Implicit Composite Kernel (ICK). ICK is flexible and can be used to include prior information in neural networks in many applications. We demonstrate the strength of our framework by showing its superior performance and flexibility on both synthetic and real-world data sets. The code is available at: [https://anonymous.4open.science/r/ICK\\_NNGP-17C5/](https://anonymous.4open.science/r/ICK_NNGP-17C5/).

## 1 Introduction

In complex regression tasks, input data often contains *multiple sources of information*. These sources can be presented in both high-dimensional (e.g. images, audios, texts, etc.) and low-dimensional (e.g. timestamps, spatial locations, etc.) forms. A common approach to learn from high-dimensional information is to use neural networks (NNs) [14, 23], as NNs are powerful enough to capture the relationship between complex high-dimensional data and target variables of interest. In many areas, NNs are standard practice, such as the dominance of Convolutional Neural Networks (CNNs) for image analysis [17, 46, 47]. In contrast, for low-dimensional information, we usually have some prior knowledge on how the information relates to the predictions. As a concrete example, consider a remote sensing problem where we predict ground measurements from satellite imagery with associated timestamps. *A priori*, we expect the ground measurements to vary periodically with respect to time between summer and winter due to seasonal effects. We would typically use a CNN to capture the complex relationship between the imagery and the ground measurements. In this case, we want to guide the learning of the CNN with our prior knowledge about the seasonality. This is

challenging because knowledge represented in NNs pertains mainly to correlation between network units instead of quantifiable statements [26].

Conversely, Gaussian processes (GPs) have been used historically to incorporate relevant prior beliefs by specifying the appropriate form of its kernel function (or covariance function) [2, 40]. One approach to modeling multiple sources of information is to assign a relevant kernel function to each source of information respectively and combine them through addition or multiplication, resulting in a *composite kernel function* [10]. This formulation means that specifying a kernel to match prior beliefs on one source of information is straightforward. Such composite kernel learning techniques are extensively used in many application areas such as multi-media data [29], neuroimaging [45], spatial data analysis, and environmental data analysis [19, 33]. In view of the clear modeling capabilities of GP, it is desirable to examine how a NN could be imbued with the same modeling ease.

In recent years, researchers have come up with a variety of methods to incorporate prior knowledge into NNs. These efforts can be broken into many categories, such as those that add prior information through loss terms like physics-informed NNs [22, 30]. Here, we focus on the major category of those methods that build integrated models of NNs and GPs with various structures [38, 42, 43]. Related to our proposed methodology, Pearce et al. [32] exploited the fact that a Bayesian neural network (BNN) approximates a GP to construct additive and multiplicative kernels, but they were limited to specific predefined kernels. Matsubara et al. [27] then resolved this limitation by constructing priors of BNN parameters based on the ridgelet transform and its dual, but they did not explicitly show how their approach works for data with multiple sources of information. To our knowledge, none of these existing approaches allows a modeler to choose any appropriate kernel of known prior information from multiple sources. We address this limitation by presenting a simple yet novel Implicit Composite Kernel (ICK) framework, which processes high-dimensional information using a kernel implicitly defined by a neural network and low-dimensional information using a chosen kernel function. The low-dimensional kernels are mapped into the neural network framework to create a straightforward and simple-to-learn implementation. Our key results and contributions are:

- We analytically show our ICK framework, under reasonable assumptions, is approximately equivalent to a Gaussian process regression (GPR) model with a composite kernel *a priori*.
- We demonstrate that our ICK framework yields better performance on both prediction and forecasting tasks even with very limited data.
- We compare to joint deep learning models, such as a neural network-random forest joint model, to show that ICK can flexibly capture the patterns of the low-dimensional information without deliberately designing a pre-processing procedure or complex NN structures.

Based on these contributions, we believe ICK will be useful in the context of learning from complex *hybrid* data with prior knowledge, especially in the field of remote sensing and spatial statistics.

## 2 Related Work

**Equivalence between NNs and GPs** The equivalence between GPs and randomly initialized single-layer NNs with infinite width was first shown by Neal [31]. With the development of modern deep learning, researchers further extended this relationship to deep networks [24, 28] and convolutional neural networks (CNNs) [11]. This relationship is crucial for proving the resemblance between GPR and our ICK framework, which will be discussed in Section 4.1.

**NNs with prior knowledge** As mentioned before, one approach to equip NNs with prior knowledge is to modify the loss function. For example, Lagaris et al. [22] solved differential equations (DEs) using NNs by setting the loss to be a function whose derivative satisfies the DE conditions. Another approach is to build integrated models of NNs and GPs. For example, Wilson et al. [43] implemented a regression network with GP priors over latent variables and made inference by approximating the posterior using Variational Bayes or sampling from the posterior using Gibbs sampling scheme. Van de Wilk et al. [38] extended GPs to high-dimensional inputs by incorporating convolutional structures into GP kernels, an approach more analogous to ICK.

**GP with composite kernels** Composite kernel GPs are widely used in both machine learning [10, 40] and geostatistical modeling [7, 12]. GPR in geostatistical modeling is also known as *kriging*

[18, 21], which serves as a surrogate model to replace expensive function evaluations. The inputs for a composite GP are usually low-dimensional (e.g. spatial distance) as GPs do not scale well with the number of samples for high-dimensional inputs [4, 5]. To overcome this issue, Pearce et al. [32] and Matsubara et al. [27] developed BNN analogue for composite GPs. Similar to these studies, our ICK framework can also be viewed as a simulation for composite GPs.

**Approximation methods for GP** For large data sets, approximation methods are needed as exact kernel learning and inference scales  $\mathcal{O}(N^3)$ . Nyström low-rank matrix approximation [8, 39] and Random Fourier Features [34, 35] are two of the most commonly used methods. A common technique is to choose inducing points as pseudo-inputs to efficiently approximate the full kernel matrix [37, 15]. Our work is inspired by these approximation techniques and we use them as *transformation functions* to map the kernel matrix into latent space representations in Section 4.2.

### 3 Background

Before elaborating on the details of our ICK framework, we introduce our notation, briefly go over the concepts of composite GPs, and describe the relationship between GPs and NNs.

#### 3.1 Problem Setup

To formalize the problem, we have a training data set which contains  $N$  data points  $\mathbf{X} = [\mathbf{x}_i]_{i=1}^N = [\mathbf{x}_1, \mathbf{x}_2, \dots, \mathbf{x}_N]^T$  and the corresponding labels of these data points are  $\mathbf{y} = [y_i]_{i=1}^N = [y_1, y_2, \dots, y_N]^T$  where  $y_i \in \mathbb{R}$ . Each data point  $\mathbf{x}_i = \{x_i^{(1)}, x_i^{(2)}, \dots, x_i^{(M)}\}$  is composed of information from  $M$  different sources where the  $m^{\text{th}}$  source of information of the  $i^{\text{th}}$  data point is denoted as  $x_i^{(m)} \in \mathbb{R}^{D_m}$ . Our goal is to learn a function  $\hat{y}_i = f(\mathbf{x}_i) : \{\mathbb{R}^{D_1}, \mathbb{R}^{D_2}, \dots, \mathbb{R}^{D_M}\} \rightarrow \mathbb{R}$  which takes in a data point  $\mathbf{x}_i$  and outputs a predicted value  $\hat{y}_i$ .

#### 3.2 Composite GPs

A Gaussian process (GP) describes a distribution over functions [40]. A key property of GP is that it can be completely defined by a mean function  $\mu(\mathbf{x})$  and a kernel function  $K(\mathbf{x}, \mathbf{x}')$ . The mean function  $\mu(\mathbf{x})$  is often assumed to be zero for simplicity. In that case, the outcome function is

$$f(\mathbf{x}) \sim \mathcal{GP}(0, K(\mathbf{x}, \mathbf{x}')). \quad (1)$$

Any finite subset of these random variables has a multivariate Gaussian distribution with mean  $\mathbf{0}$  and kernel matrix  $\mathbf{K}$  whose entries can be calculated as  $\mathbf{K}_{ij} = K(\mathbf{x}_i, \mathbf{x}_j)$ . In many situations, the full kernel function is built by a composite kernel by combining simple kernels through addition  $K_{\text{comp}}(\mathbf{x}, \mathbf{x}') = K_1(\mathbf{x}, \mathbf{x}') + K_2(\mathbf{x}, \mathbf{x}')$  or multiplication  $K_{\text{comp}}(\mathbf{x}, \mathbf{x}') = K_1(\mathbf{x}, \mathbf{x}')K_2(\mathbf{x}, \mathbf{x}')$  [10]. A useful property that ICK exploits is that  $K_1$  and  $K_2$  can take different subparts of  $\mathbf{x}$  as their inputs. For example,  $K_{\text{comp}}(\mathbf{x}, \mathbf{x}') = K_1(x^{(1)}, x^{(1)'}) + K_2(x^{(2)}, x^{(2)'})$  or  $K_{\text{comp}}(\mathbf{x}, \mathbf{x}') = K_1(x^{(1)}, x^{(1)'})K_2(x^{(2)}, x^{(2)'})$ . Other methods such as functional mapping are also valid if the resulting kernel matrix  $\mathbf{K}$  is positive semidefinite (PSD) for all possible choices of data set  $\mathbf{X}$  [36].

#### 3.3 Correspondence between GPs and NNs

Neal [31] proved that a single-hidden layer network with infinite width is *exactly equivalent* to a GP over data indices  $i = 1, 2, \dots, N$  under the assumption that the weight and bias parameters of the hidden layer are i.i.d. Gaussian with zero mean. Lee et al. [24] and Garriga et al. [11] then extended this statement to deep neural networks and convolutional neural networks (CNNs), respectively. However, if the width (or the number of channels) of a network is finite, then these results state that the network *approximately* converges to a GP with zero mean as in the following lemma.

**Lemma 1** Let  $\mathbf{z} = f_{\text{NN}}(x^{(1)}) : \mathbb{R}^{D_1} \rightarrow \mathbb{R}^p$  be the latent representation extracted from  $x^{(1)}$  where  $p$  is the dimension of the extracted representation and  $f_{\text{NN}}$  is a neural network with finite width and zero-mean i.i.d. parameters. The  $k^{\text{th}}$  entry of this representation will approximately follow a

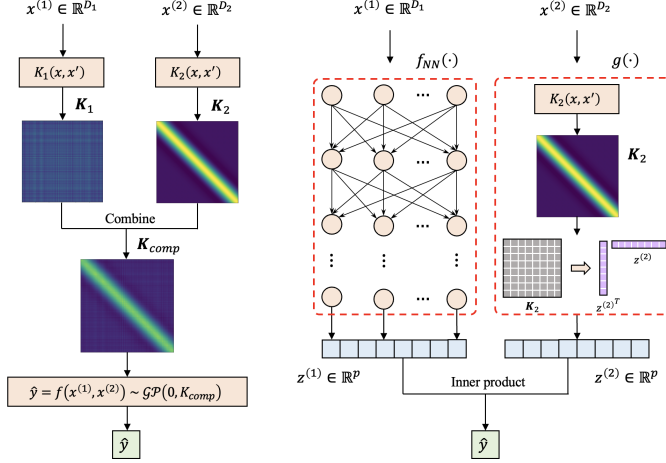


Figure 1: Given data containing 2 sources of information  $x^{(1)}$  and  $x^{(2)}$ , we can process the data using either **(Left)** a composite Gaussian process regression (GPR) model or **(Right)** our ICK framework where  $x^{(1)}$  is processed with a neural network  $f_{NN}(\cdot)$  and  $x^{(2)}$  is processed with  $g(\cdot)$  where  $g(\cdot)$  consists of a kernel function  $K_2$  and some transformation which maps the kernel matrix  $K_2$  into the latent space.

#### NN-implied GP

$$z_k = f_{NN}(x^{(1)})_k \sim \mathcal{GP}_{approx}(0, K_{NN}(x^{(1)}, x^{(1)'})). \quad (2)$$

That is to say, the  $k^{th}$  component  $z_k$  of the representation extracted by the network has zero mean  $\mathbb{E}_{p(\theta^{(1)})}[z_{ik}^{(1)}] = 0$  for all  $i = 1, 2, \dots, N$  where  $\theta$  represents the network parameters. The covariance between  $z_{ik}^{(1)}$  and  $z_{jk}^{(1)}$  for *different* data indices  $i, j = 1, 2, \dots, N$  can be approximated as  $\text{cov}(z_{ik}^{(1)}, z_{jk}^{(1)}) = \mathbb{E}_{p(\theta^{(1)})}[z_{ik}^{(1)} z_{jk}^{(1)}] \approx K_{NN}(x_i^{(1)}, x_j^{(1)})$  where  $x_i^{(1)}$  and  $x_j^{(1)}$  are the corresponding inputs for the network and  $K_{NN}$  is the kernel function implied by the network.

## 4 Implicit Composite Kernel (ICK) Framework

We show the structure of a composite GPR model and our ICK framework in Figure 1. To make the illustration clear, we limit ourselves to data with information from 2 different sources  $x = \{x^{(1)}, x^{(2)}\}$  where  $x^{(1)}$  is high-dimensional and  $x^{(2)}$  is low-dimensional (i.e.  $D_1 \gg D_2$ ) with some known relationship with the target  $y$ . We are inspired by composite GPR, which computes 2 different kernel matrices  $K_1$  and  $K_2$  and then combines them into a single composite kernel matrix  $K_{comp}$ . However, as discussed before, it is more suitable to use a NN to learn from the high dimensional information  $x^{(1)}$ . In our ICK framework, we process  $x^{(1)}$  with a NN  $f_{NN}(\cdot) : \mathbb{R}^{D_1} \rightarrow \mathbb{R}^p$  and  $x^{(2)}$  with a mapping  $g(\cdot) : \mathbb{R}^{D_2} \rightarrow \mathbb{R}^p$  which consists of a kernel function  $K_2$  followed by a kernel-to-latent-space transformation (described in Section 4.2), resulting in two latent representations  $z^{(1)}, z^{(2)} \in \mathbb{R}^p$ . Then, we make a prediction  $\hat{y}$  by doing an *inner product* between these two representations  $\hat{y} = f_{NN}(x^{(1)}) \cdot g(x^{(2)})$ . Finally, the parameters of both the NN and the kernel function are learned via gradient-based optimization methods [3, 20].

In the sections below, we first analytically show that our ICK framework is *approximately* equivalent to a composite GPR model *a priori* using a multiplicative kernel between the kernel implicitly defined by the NN on  $x^{(1)}$  and the chosen kernel on  $x^{(2)}$ . We then show how we implement the kernel-to-latent-space transformation in detail. Here, we note that we apply ICK for multiplicative kernels but note that an additive kernel may be constructed using the methods of Pearce et al. [32].

### 4.1 Resemblance between Composite GPR and ICK

We will analytically prove the following theorem for data with information from 2 different sources  $x = \{x^{(1)}, x^{(2)}\}$  for clarity, and we note this theorem can be straightforwardly extended to  $M > 2$ .

**Theorem 1** Let  $f_{NN} : \mathbb{R}^{D_1} \rightarrow \mathbb{R}^p$  be a NN-implied function and  $g : \mathbb{R}^{D_2} \rightarrow \mathbb{R}^p$  be a mapping function, and define an inner product  $\hat{y}$  between the representations  $z^{(1)} = f_{NN}(x^{(1)})$  and  $z^{(2)} =$

$g(x^{(2)})$ . Then this inner product approximately follows a composite GPR model

$$\hat{y} = f_{ICK}(x^{(1)}, x^{(2)}) = f_{NN}(x^{(1)}) \cdot g(x^{(2)}) \sim \mathcal{GP}_{approx}(0, K_{NN}^{(1)} K^{(2)}), \quad (3)$$

if  $g$  includes the following deterministic kernel-to-latent-space transformation

$$K^{(2)}(x_i^{(2)}, x_j^{(2)}) \approx \mathbf{z}_i^{(2)T} \mathbf{z}_j^{(2)} = g(x_i^{(2)})^T g(x_j^{(2)}), \quad (4)$$

where  $K_{NN}^{(1)}$  is a NN-implied kernel and  $K^{(2)}$  is any valid kernel of our choice.

To prove Theorem 1, we first make the following assumption.

**Assumption 1** For latent representations  $\mathbf{z}_i^{(m)}$  and  $\mathbf{z}_j^{(m)}$  extracted from different data points  $\mathbf{x}_i$  and  $\mathbf{x}_j$  where  $i \neq j$  and  $m \in \{1, 2\}$ , the interactions between different entries of  $\mathbf{z}_i^{(m)}$  and  $\mathbf{z}_j^{(m)}$  can be reasonably ignored. In other words, let  $\theta^{(m)}$  be the parameters of the network or the kernel function which takes in  $x^{(m)}$  and outputs  $\mathbf{z}^{(m)}$ , we have  $\mathbb{E}_{p(\theta^{(m)})} [z_{ik}^{(m)} z_{jl}^{(m)}] = 0$  for all  $k \neq l$ .

With Assumption 1 and Lemma 1, let  $\Theta = \{\theta^{(1)}, \theta^{(2)}\}$  represent the parameters of the ICK framework, we can calculate the covariance between  $\hat{y}_i$  and  $\hat{y}_j$  for different data indices  $i \neq j$  as follows

$$\text{cov}(\hat{y}_i, \hat{y}_j) = \mathbb{E}_{p(\Theta)}[\hat{y}_i \hat{y}_j] - \mathbb{E}_{p(\Theta)}[\hat{y}_i] \mathbb{E}_{p(\Theta)}[\hat{y}_j] \quad (5)$$

$$= \mathbb{E}_{p(\Theta)} \left[ \left( \sum_{k=1}^p z_{ik}^{(1)} z_{ik}^{(2)} \right) \left( \sum_{k=1}^p z_{jk}^{(1)} z_{jk}^{(2)} \right) \right] \quad (6)$$

$$= \mathbb{E}_{p(\Theta)} \left[ \sum_{k=1}^p \sum_{l=1}^p z_{ik}^{(1)} z_{jl}^{(1)} z_{ik}^{(2)} z_{jl}^{(2)} \right] \quad (7)$$

$$= \mathbb{E}_{p(\Theta)} \left[ \sum_{k=1}^p z_{ik}^{(1)} z_{jk}^{(1)} z_{ik}^{(2)} z_{jk}^{(2)} \right] \quad (8)$$

$$= \sum_{k=1}^p \mathbb{E}_{p(\theta^{(1)})} [z_{ik}^{(1)} z_{jk}^{(1)}] \mathbb{E}_{p(\theta^{(2)})} [z_{ik}^{(2)} z_{jk}^{(2)}] \quad (9)$$

$$\approx K_{NN}^{(1)}(x_i^{(1)}, x_j^{(1)}) \sum_{k=1}^p \mathbb{E}_{p(\theta^{(2)})} [z_{ik}^{(2)} z_{jk}^{(2)}]. \quad (10)$$

Here, from Equation 5 to Equation 6, we use the statement  $\mathbb{E}_{p(\theta^{(1)})} [z_{ik}^{(1)}] = 0$  from Lemma 1 and the independence between  $\theta^{(1)}$  and  $\theta^{(2)}$ , which leads to  $\mathbb{E}_{p(\Theta)}[\hat{y}_i] = \mathbb{E}_{p(\Theta)}[\hat{y}_j] = 0$ . From Equation 7 to Equation 8, we get rid of all the cross terms under Assumption 1. From Equation 8 to Equation 9, we again make use of the independence between  $\theta^{(1)}$  and  $\theta^{(2)}$ . From Equation 9 to Equation 10, we use the statement  $\mathbb{E}_{p(\theta^{(1)})} [z_{ik}^{(1)} z_{jk}^{(1)}] \approx K_{NN}(x_i^{(1)}, x_j^{(1)})$  from Lemma 1. If the kernel-to-latent-space transformation in  $g(\cdot)$  is *deterministic*, we can remove the expectation sign from the summation term in Equation 10 and the covariance can be further expressed as

$$\text{cov}(\hat{y}_i, \hat{y}_j) \approx K_{NN}^{(1)}(x_i^{(1)}, x_j^{(1)}) \left( \mathbf{z}_i^{(2)T} \mathbf{z}_j^{(2)} \right) = K_{NN}^{(1)}(x_i^{(1)}, x_j^{(1)}) K^{(2)}(x_i^{(2)}, x_j^{(2)}), \quad (11)$$

which means that  $\hat{y}$  approximately follows a GP with composite kernel  $K_{\text{comp}}(\mathbf{x}_i, \mathbf{x}_j) = K_{NN}^{(1)}(x_i^{(1)}, x_j^{(1)}) K^{(2)}(x_i^{(2)}, x_j^{(2)})$  *a priori*. This completes our proof of Theorem 1.

## 4.2 Kernel-to-latent-space Transformation

We now show how we can construct an appropriate mapping  $g(\cdot)$  with the necessary properties. Here we adopt two methods, Nyström approximation and Random Fourier Features (RFF), to map the kernel matrix into the latent space. Below, we give the formulations and results for the Nyström method, and give the methods and results for RFF in Appendix B. According to Yang et al. [44], the Nyström method will yield much better performance than RFF if there exists a large gap in the eigen-spectrum of the kernel matrix. In our applications, we also observe a large eigen-gap (see details in Appendix C) and Nyström method does generalize much better than RFF. We name our framework with Nyström method and random Fourier Features ICKy and ICKr, respectively.

#### 4.2.1 Nyström Method

The main idea of Nyström method [39] is to approximate the kernel matrix  $\mathbf{K} \in \mathbb{R}^{N \times N}$  with a much smaller low-rank matrix  $\mathbf{K}_q \in \mathbb{R}^{q \times q}$  where  $q \ll N$  so both the computational and space complexity of kernel learning can be significantly reduced

$$\mathbf{K} \approx \hat{\mathbf{K}} = \mathbf{K}_{nq} \mathbf{K}_q^{-1} \mathbf{K}_{nq}^T. \quad (12)$$

The entries of  $\mathbf{K}_q$  and  $\mathbf{K}_{nq}$  can be calculated as  $(\mathbf{K}_q)_{ij} = K(\hat{x}_i, \hat{x}_j), i, j \in \{1, 2, \dots, q\}$  and  $(\mathbf{K}_{nq})_{ij} = K(x_i, \hat{x}_j), i \in \{1, 2, \dots, N\}, j \in \{1, 2, \dots, q\}$ , respectively.  $x$  represents the original data points and  $\hat{x}$  represents pre-defined integrating points (or pseudo-inputs [37]). In our study, these integrating points are chosen by defining an evenly spaced vector over the range of original data points. By performing Cholesky decomposition  $\mathbf{K}_q^{-1} = \mathbf{U}^T \mathbf{U}$ , where  $\mathbf{U} \in \mathbb{R}^{q \times q}$ ,  $\hat{\mathbf{K}}$  is

$$\hat{\mathbf{K}} = \mathbf{K}_{nq} \mathbf{K}_q^{-1} \mathbf{K}_{nq}^T = \mathbf{K}_{nq} \mathbf{U}^T \mathbf{U} \mathbf{K}_{nq}^T = \left( \mathbf{U} \mathbf{K}_{nq}^T \right)^T \left( \mathbf{U} \mathbf{K}_{nq}^T \right). \quad (13)$$

Therefore, if we set the number of integrating points to be  $q = p$ , then we can use  $\mathbf{z}_i \triangleq \mathbf{U} \left( \mathbf{K}_{np}^T \right)_{:,i}$  as a kernel-to-latent-space transformation because each element in  $\mathbf{K}$  satisfies the necessary property we state in Theorem 1:  $K(x_i, x_j) = K_{ij} \approx \hat{K}_{ij} = \mathbf{z}_i^T \mathbf{z}_j$ . Conveniently, modern deep learning frameworks can propagate gradients through the Cholesky operation, making it straightforward to update the kernel parameters with gradient methods. Note that as we increase the number of integrating points  $p$ , the approximation error between  $\mathbf{K}$  and  $\hat{\mathbf{K}}$  decreases. However, it is not recommended to set  $p$  very large as updating the Cholesky decomposition requires  $\mathcal{O}(p^3)$  and computing  $\hat{\mathbf{K}}$  scales  $\mathcal{O}(p^2)$  per data point. The empirical impact of  $p$  is shown in Appendix E.

## 5 Experimental Results

We evaluate ICKy on 3 different data sets: a synthetic data set, a remote sensing data set, and a data set obtained from UCI Machine Learning Repository [9]. Note that in all the 3 experiments, our ICKy framework only consists of 2 kernels (i.e.  $M = 2$ ), one NN-implied kernel and one chosen kernel function with trainable parameters. To verify that ICKy can work with more than 2 kernels, we create another synthetic data set with 3 kernels and show the corresponding results in Appendix A. In addition, the experimental results for ICKr is provided in Appendix B. All experiments are conducted on a computer cluster equipped with a GeForce RTX 2080 Ti GPU.

### 5.1 Synthetic Data

To verify that ICKy can simulate a *multiplicative kernel*, we create a synthetic data set  $y \sim \mathcal{GP}(0, K_1 K_2)$  containing 3000 data points where  $x^{(1)} \in [0, 1]$  is the input for the linear kernel  $K_1$  and  $x^{(2)} \in [0, 2]$  is the input for the *spectral mixture* kernel [41]  $K_2$  with 2 components. With ICKy, we process  $x^{(1)}$  with a single-hidden-layer NN and  $x^{(2)}$  with a spectral mixture kernel function. We evaluate ICKy on both a *prediction* task (where we first randomly shuffle the data points and do a 50:50 train-test split) and a *forecasting* task (where we use only the data points with  $x^{(2)} < 0.6$  for training and the rest for testing).

We first examine whether ICKy can retrieve the spectral mixture kernel in the prediction task. After fitting the parameters of the spectral mixture kernel in ICKy, we compute the kernel matrix  $\mathbf{K}_{\text{ICKy}}$  using these learned parameters and compare it with the true kernel matrix  $\mathbf{K}_{\text{true}}$  by calculating the absolute difference between them as displayed in Figure 2. As can be observed,  $\mathbf{K}_{\text{ICKy}}$  and  $\mathbf{K}_{\text{true}}$  are similar and their absolute difference is relatively small, indicating that ICKy can approximately retrieve the spectral mixture kernel.

We then compare ICKy with two models: a plain multi-layer perceptron (MLP) applied to the concatenated features and a novel multi-layer perceptron-random forest (MLP-RF) joint model employed by Zheng et al. [46] where MLP learns from  $x^{(1)}$  and RF learns from  $x^{(2)}$ . We believe MLP-RF serves as a good benchmark model as it is a joint model with similar architecture to our ICKy framework. To see how ICKy simulates the spectral mixture kernel, we plot only  $x^{(2)}$  against the predicted value of  $y$  as shown in Figure 3. As can be seen from the figure, in the prediction task

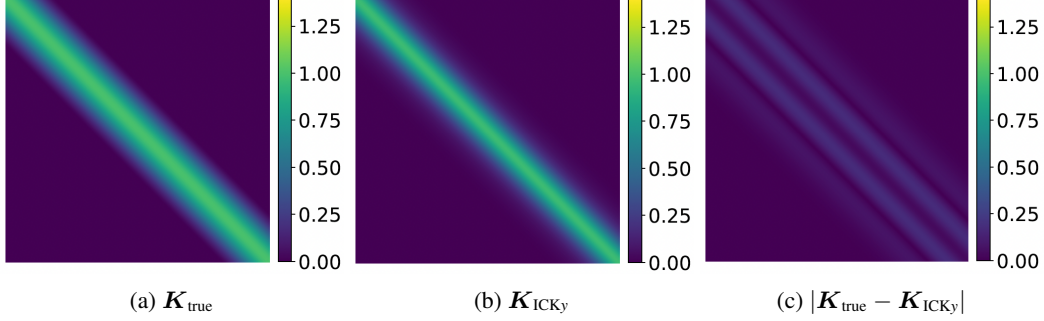


Figure 2: Visualization of (a) True matrix (b) estimated matrix by our ICKy framework, and (c) absolute difference between the true and estimated matrix for the spectral mixture kernel

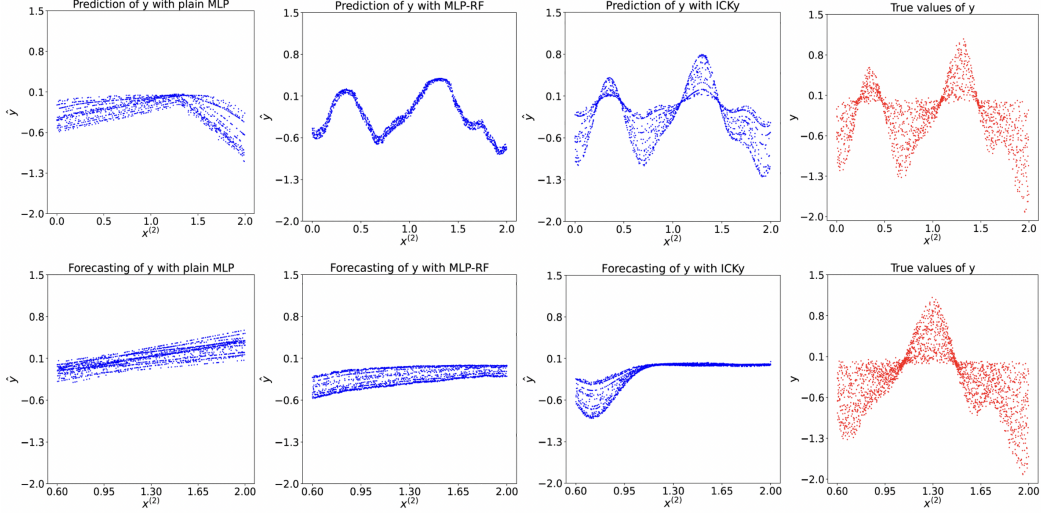


Figure 3: Prediction (top row) and forecasting (bottom row) of  $y \sim \mathcal{GP}(0, K_1 K_2)$ , where  $x^{(1)}$  is input to a linear kernel  $K_1$  and  $x^{(2)}$  is input to a spectral mixture kernel  $K_2$ . We plot  $x^{(2)}$  against the predicted  $y$ . We show results from a plain MLP (left column), MLP-RF (middle left column), and ICKy framework (middle right column), and we compare to the true values of  $y$  (right column).

(top row), plain MLP only captures the linear trend. MLP-RF only captures the mean of the spectral mixture components. In contrast, our ICKy framework captures both the mean and the variance of the spectral mixture kernel. In the forecasting task (bottom row), ICKy also outperforms plain MLP and MLP-RF as it approximately captures the rising trend in the range of  $x^{(2)} \in [0.6, 1]$ . When  $x^{(2)} > 1$ , ICKy is unable to confidently extrapolate, so it starts to "fail gracefully" by reverting to the mean value of  $y$  (near zero), which we view as a favorable functional property.

We also test plain MLP, MLP-RF, and ICKy on the prediction task using different number of training samples. As displayed in Figure 4, ICKy yields the smallest error among all the 3 frameworks even with very limited data. In addition, to test the robustness of ICKy, we conduct the same experiments on another synthetic data set in Appendix D to confirm that ICKy can simulate an *additive kernel*.

## 5.2 Remote Sensing Data

We believe ICKy will be particularly useful for remote sensing applications. In this experiment, we collect remote sensing data from 51 air quality monitoring (AQM) stations located in the National Capital Territory (NCT) of Delhi and its satellite cities over the period from January 1, 2018 to June 30, 2020 (see Appendix F for notes on data availability). Each data point  $x = \{x, t\}$  contains 2 sources of information: a three-band natural color (red-blue-green) satellite image  $x$  as the high-dimensional information and the corresponding timestamp as the low-dimensional information. Note that we

convert the timestamps into numerical values  $t$  (where the day 2018-01-01 corresponds to  $t = 0$ ) before feeding them into the models. Our goal is to predict the ground-level  $\text{PM}_{2.5}$  concentration  $\hat{y} = f(x, t)$  using both sources of information.

We split the train and test data set based on  $t$ . Specifically, we use all the data points with  $t \geq 500$  for testing and the rest for training. As  $\text{PM}_{2.5}$  varies with time on a yearly basis, we use an *exponential-sine-squared* kernel with a period of  $T = 365$  (days) to process the low-dimensional information  $t$ . The satellite images are processed with a two-layer CNN. We then compare ICKy with 2 benchmarks: a Convolutional Neural Network-Random Forest (CNN-RF) joint model [46, 47] (similar to the MLP-RF model in Section 5.1, where RF learns the temporal variation of  $\text{PM}_{2.5}$  and CNN captures the spatial variation of  $\text{PM}_{2.5}$  from satellite images) and a *carefully designed* CNN-RF model that maps  $t$  into two new features,  $\sin(2\pi t/365)$  and  $\cos(2\pi t/365)$ , to explicitly model seasonality.

Figure 5 shows the true versus the forecasted  $\text{PM}_{2.5}$  values by both ICKy and the other 2 benchmarks. It can be observed that ICKy outperforms both benchmarks with the highest correlation coefficients and the lowest errors on the forecasting task. Specifically, CNN-RF joint model fails to forecast  $\text{PM}_{2.5}$  as shown in Figure 5a. After including seasonality, CNN-RF performs significantly better as shown in Figure 5b, but the forecasted  $\text{PM}_{2.5}$  values are still less smooth than those from ICKy (Figure 5c) due to the discontinuous nature of the RF regressor [6, 13]. We also visualize these results in the form of time series in Appendix F.

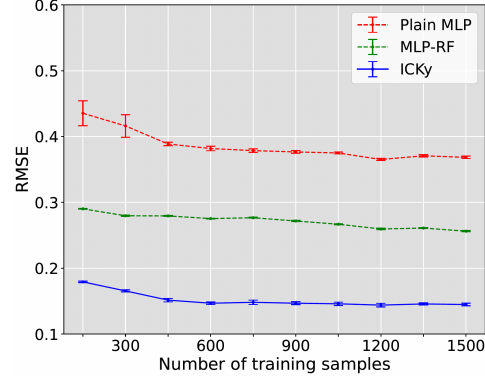


Figure 4: Prediction error of plain MLP, MLP-RF, and ICKy with different amount of training data generated by  $y = \mathcal{GP}(0, K_1 K_2)$ .

### 5.3 UCI Machine Learning Repository Data

To see if our ICKy framework generalizes to other domains, we acquire another data set containing the normalized productivity and corresponding features of garment workers from the UCI Machine Learning Repository. Imran et al. [1] employed a dense MLP with 2 hidden layers to predict the worker productivity with collected features such as date, team number, targeted productivity, etc. To test our ICKy framework, we separate out the *date* and use it as the low-dimensional information. The rest of the features (excluding the temporal information) are then concatenated together to serve as the high-dimensional information. Observing that the *daily averaged* worker productivity has an approximate *monthly trend*, we again use an *exponential-sine-squared* kernel. The network architecture of ICKy is the same as that of the two-hidden-layer MLP benchmark. Based on the results shown in Table 1, ICKy has the best performance when the period parameter of the kernel is set to be  $T = 30$  (days) and it outperforms the plain MLP benchmark by almost **one order of magnitude**. When we set  $T = 2$  or  $T = 7$ , this improvement is less significant, which aligns with our initial observation that the daily averaged productivity has a monthly seasonal trend.

Table 1: Prediction error of actual worker productivity on the test data set with dense MLP and ICKy with different period parameters

	MLP [1]	ICKy $T = 2$	ICKy $T = 7$	ICKy $T = 30$
MSE	0.018	$0.00365 \pm 0.00142$	$0.00048 \pm 0.00012$	<b><math>0.00035 \pm 0.00010</math></b>
MAE	0.086	$0.04984 \pm 0.01083$	$0.01475 \pm 0.00152$	<b><math>0.01240 \pm 0.00176</math></b>
MAPE	15.932	$6.587 \pm 1.418$	$2.239 \pm 0.246$	<b><math>1.959 \pm 0.301</math></b>

## 6 Discussion

**Efficiency, Flexibility, and Generalization** Compared to exact composite GP models which scale  $\mathcal{O}(N^3)$ , the training process of our ICK framework is more efficient as it leverages standard back-propagation to learn both the paramters of NN and the kernel function. In addition, the network architecture of ICK can be very simple, as can be seen in all 3 experiments of ours, which further



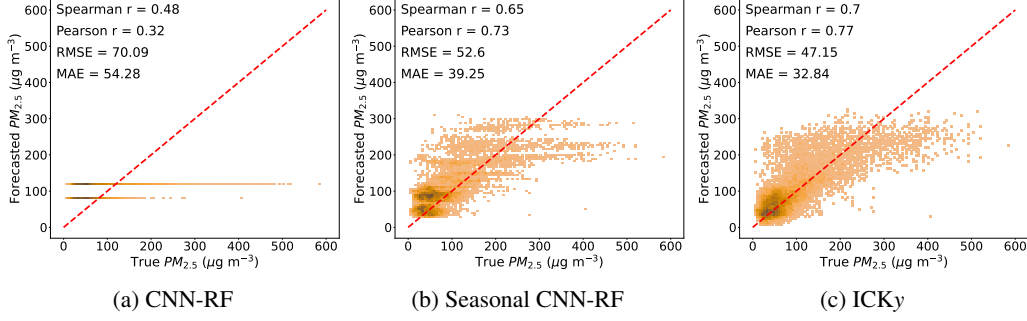


Figure 5: Density plots of the true  $PM_{2.5}$  concentrations against the **forecasted**  $PM_{2.5}$  concentrations for  $t \geq 500$  using (a) a CNN-RF joint model [46, 47], (b) a CNN-RF joint model with seasonality incorporated, and (c) our ICKy framework

reduces its time and space complexity. Besides efficiency, our ICK framework is more flexible compared to other joint models (i.e. BNNs and CNN-RF). To be specific, the BNNs implemented by Pearce et al. [32] cannot simulate complicated kernels such as the spectral mixture kernel we use in Section 5.1. The CNN-RF joint model implemented by Zheng et al. [46] requires us to carefully design the input pre-processing procedure. Also, ICK generalizes well to unseen data even with very limited training samples.

**Limitations** A major limitation of ICK lies in our method of combining latent representations as the nature of inner product (i.e. the effect of multiplying small numbers) may cause *vanishing gradient* problems when we have a large number of sources of information (i.e.  $M$  is large). Furthermore, this paper only discusses the theoretical relationship between ICK and composite GPR *a priori*. This relationship will not exactly hold true *a posteriori*, although empirical results [24] and theoretical results [16] in slightly different contexts suggest that they may be close. Future work will evaluate this gap.

**Broader Impacts** We believe our framework is extensively applicable to regression problems in many fields of study involving high-dimensional data and multiple sources of information with perceptible trends, such as remote sensing, spatial statistics, or clinical diagnosis.

## 7 Conclusion

This paper presents a novel yet surprisingly simple Implicit Composite Kernel (ICK) framework to learn from *hybrid* data containing both high-dimensional information and low-dimensional information with prior knowledge. We first analytically show the resemblance between ICK and composite GPR models and then conduct experiments using both synthetic and real-world data. It appears that ICK outperforms various benchmark models in our experiments with lowest prediction errors and highest correlations even with very limited data. Overall, we show that our ICK framework is exceptionally powerful when learning from *hybrid* data with our prior knowledge incorporated, and we hope our work can inspire more future research on joint machine learning models, enhancing their performance, efficiency, flexibility, and generalization capability.

## References

- [1] Abdullah Al Imran, Md Nur Amin, Md Rifatul Islam Rifat, and Shamprikta Mehreen. Deep neural network approach for predicting the productivity of garment employees. In *2019 6th International Conference on Control, Decision and Information Technologies (CoDIT)*, pages 1402–1407. IEEE, 2019.
- [2] Christopher M Bishop and Nasser M Nasrabadi. *Pattern recognition and machine learning*, volume 4. Springer, 2006.
- [3] Léon Bottou, Frank E Curtis, and Jorge Nocedal. Optimization methods for large-scale machine learning. *Siam Review*, 60(2):223–311, 2018.

- [4] Mohamed A Bouhlel and Joaquim RRA Martins. Gradient-enhanced kriging for high-dimensional problems. *Engineering with Computers*, 35(1):157–173, 2019.
- [5] Mohamed Amine Bouhlel, Nathalie Bartoli, Abdelkader Otsmane, and Joseph Morlier. Improving kriging surrogates of high-dimensional design models by partial least squares dimension reduction. *Structural and Multidisciplinary Optimization*, 53(5):935–952, 2016.
- [6] Leo Breiman. Random forests. *Machine learning*, 45(1):5–32, 2001.
- [7] Abhirup Datta, Sudipto Banerjee, Andrew O Finley, and Alan E Gelfand. Hierarchical nearest-neighbor gaussian process models for large geostatistical datasets. *Journal of the American Statistical Association*, 111(514):800–812, 2016.
- [8] Petros Drineas, Michael W Mahoney, and Nello Cristianini. On the nyström method for approximating a gram matrix for improved kernel-based learning. *journal of machine learning research*, 6(12), 2005.
- [9] Dheeru Dua and Casey Graff. UCI machine learning repository, 2017.
- [10] David Duvenaud. *Automatic model construction with Gaussian processes*. PhD thesis, University of Cambridge, 2014.
- [11] Adrià Garriga-Alonso, Carl Edward Rasmussen, and Laurence Aitchison. Deep convolutional networks as shallow gaussian processes. *arXiv preprint arXiv:1808.05587*, 2018.
- [12] Alan E Gelfand and Erin M Schliep. Spatial statistics and gaussian processes: A beautiful marriage. *Spatial Statistics*, 18:86–104, 2016.
- [13] Pierre Geurts, Damien Ernst, and Louis Wehenkel. Extremely randomized trees. *Machine learning*, 63(1):3–42, 2006.
- [14] Ian Goodfellow, Yoshua Bengio, and Aaron Courville. *Deep learning*. MIT press, 2016.
- [15] James Hensman, Nicolo Fusi, and Neil D Lawrence. Gaussian processes for big data. *arXiv preprint arXiv:1309.6835*, 2013.
- [16] Arthur Jacot, Franck Gabriel, and Clément Hongler. Neural tangent kernel: Convergence and generalization in neural networks. *Advances in neural information processing systems*, 31, 2018.
- [17] Ziyang Jiang, Tongshu Zheng, Mike Bergin, and David Carlson. Improving spatial variation of ground-level pm<sub>2.5</sub> prediction with contrastive learning from satellite imagery. *Science of Remote Sensing*, page 100052, 2022.
- [18] Andre G Journel and Charles J Huijbregts. *Mining geostatistics*. The Blackburn Press, 1976.
- [19] Hyoung-Moon Kim, Bani K Mallick, and Chris C Holmes. Analyzing nonstationary spatial data using piecewise gaussian processes. *Journal of the American Statistical Association*, 100(470):653–668, 2005.
- [20] Diederik P Kingma and Jimmy Ba. Adam: A method for stochastic optimization. *arXiv preprint arXiv:1412.6980*, 2014.
- [21] Daniel G Krige. A statistical approach to some basic mine valuation problems on the witwatersrand. *Journal of the Southern African Institute of Mining and Metallurgy*, 52(6):119–139, 1951.
- [22] Isaac E Lagaris, Aristidis Likas, and Dimitrios I Fotiadis. Artificial neural networks for solving ordinary and partial differential equations. *IEEE transactions on neural networks*, 9(5):987–1000, 1998.
- [23] Yann LeCun, Yoshua Bengio, and Geoffrey Hinton. Deep learning. *nature*, 521(7553):436–444, 2015.
- [24] Jaehoon Lee, Yasaman Bahri, Roman Novak, Samuel S Schoenholz, Jeffrey Pennington, and Jascha Sohl-Dickstein. Deep neural networks as gaussian processes. *arXiv preprint arXiv:1711.00165*, 2017.
- [25] Chris J Maddison, Andriy Mnih, and Yee Whye Teh. The concrete distribution: A continuous relaxation of discrete random variables. *arXiv preprint arXiv:1611.00712*, 2016.
- [26] Gary Marcus. Deep learning: A critical appraisal. *arXiv preprint arXiv:1801.00631*, 2018.

- [27] Takuo Matsubara, Chris J Oates, and François-Xavier Briol. The ridgelet prior: A covariance function approach to prior specification for bayesian neural networks. *arXiv preprint arXiv:2010.08488*, 2020.
- [28] Alexander G de G Matthews, Mark Rowland, Jiri Hron, Richard E Turner, and Zoubin Ghahramani. Gaussian process behaviour in wide deep neural networks. *arXiv preprint arXiv:1804.11271*, 2018.
- [29] Brian McFee, Gert Lanckriet, and Tony Jebara. Learning multi-modal similarity. *Journal of machine learning research*, 12(2), 2011.
- [30] Ben Moseley, Andrew Markham, and Tarje Nissen-Meyer. Solving the wave equation with physics-informed deep learning. *arXiv preprint arXiv:2006.11894*, 2020.
- [31] Radford M Neal. Priors for infinite networks. In *Bayesian Learning for Neural Networks*, pages 29–53. Springer, 1996.
- [32] Tim Pearce, Russell Tsuchida, Mohamed Zaki, Alexandra Brintrup, and Andy Neely. Expressive priors in bayesian neural networks: Kernel combinations and periodic functions. In *Uncertainty in artificial intelligence*, pages 134–144. PMLR, 2020.
- [33] Dejan Petelin, Alexandra Grancarova, and Juš Kocijan. Evolving gaussian process models for prediction of ozone concentration in the air. *Simulation modelling practice and theory*, 33:68–80, 2013.
- [34] Ali Rahimi and Benjamin Recht. Random features for large-scale kernel machines. *Advances in neural information processing systems*, 20, 2007.
- [35] Ali Rahimi and Benjamin Recht. Weighted sums of random kitchen sinks: Replacing minimization with randomization in learning. *Advances in neural information processing systems*, 21, 2008.
- [36] John Shawe-Taylor, Nello Cristianini, et al. *Kernel methods for pattern analysis*. Cambridge university press, 2004.
- [37] Edward Snelson and Zoubin Ghahramani. Sparse gaussian processes using pseudo-inputs. *Advances in neural information processing systems*, 18, 2005.
- [38] Mark Van der Wilk, Carl Edward Rasmussen, and James Hensman. Convolutional gaussian processes. *Advances in Neural Information Processing Systems*, 30, 2017.
- [39] Christopher Williams and Matthias Seeger. Using the nyström method to speed up kernel machines. *Advances in neural information processing systems*, 13, 2000.
- [40] Christopher K Williams and Carl Edward Rasmussen. *Gaussian processes for machine learning*, volume 2. MIT press Cambridge, MA, 2006.
- [41] Andrew Wilson and Ryan Adams. Gaussian process kernels for pattern discovery and extrapolation. In *International conference on machine learning*, pages 1067–1075. PMLR, 2013.
- [42] Andrew Gordon Wilson, Zhiting Hu, Ruslan Salakhutdinov, and Eric P Xing. Deep kernel learning. In *Artificial intelligence and statistics*, pages 370–378. PMLR, 2016.
- [43] Andrew Gordon Wilson, David A Knowles, and Zoubin Ghahramani. Gaussian process regression networks. *arXiv preprint arXiv:1110.4411*, 2011.
- [44] Tianbao Yang, Yu-Feng Li, Mehrdad Mahdavi, Rong Jin, and Zhi-Hua Zhou. Nyström method vs random fourier features: A theoretical and empirical comparison. *Advances in neural information processing systems*, 25, 2012.
- [45] Daoqiang Zhang, Yaping Wang, Luping Zhou, Hong Yuan, Dinggang Shen, Alzheimer’s Disease Neuroimaging Initiative, et al. Multimodal classification of alzheimer’s disease and mild cognitive impairment. *Neuroimage*, 55(3):856–867, 2011.
- [46] Tongshu Zheng, Michael Bergin, Guoyin Wang, and David Carlson. Local pm2. 5 hotspot detector at 300 m resolution: A random forest–convolutional neural network joint model jointly trained on satellite images and meteorology. *Remote Sensing*, 13(7):1356, 2021.
- [47] Tongshu Zheng, Michael H Bergin, Shijia Hu, Joshua Miller, and David E Carlson. Estimating ground-level pm2. 5 using micro-satellite images by a convolutional neural network and random forest approach. *Atmospheric Environment*, 230:117451, 2020.

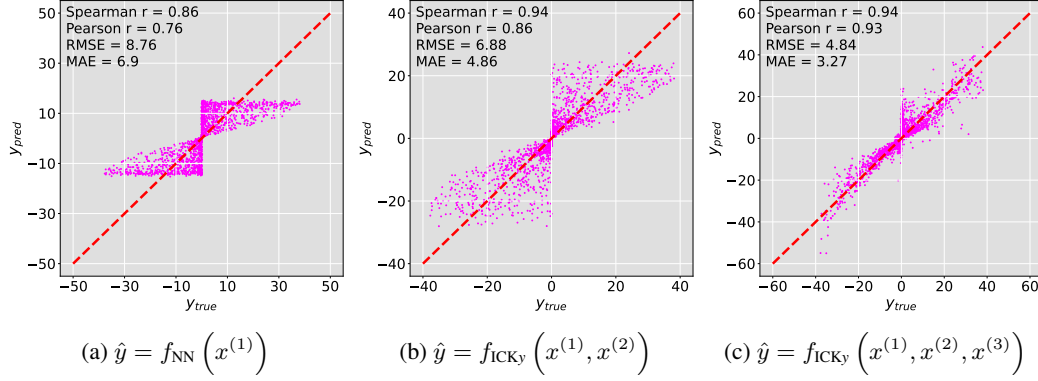


Figure A1: Scatter plots of the true values of  $y$  against the predicted values of  $y$  using our ICKy framework with (a) one source, (b) 2 sources, and (c) 3 sources of information

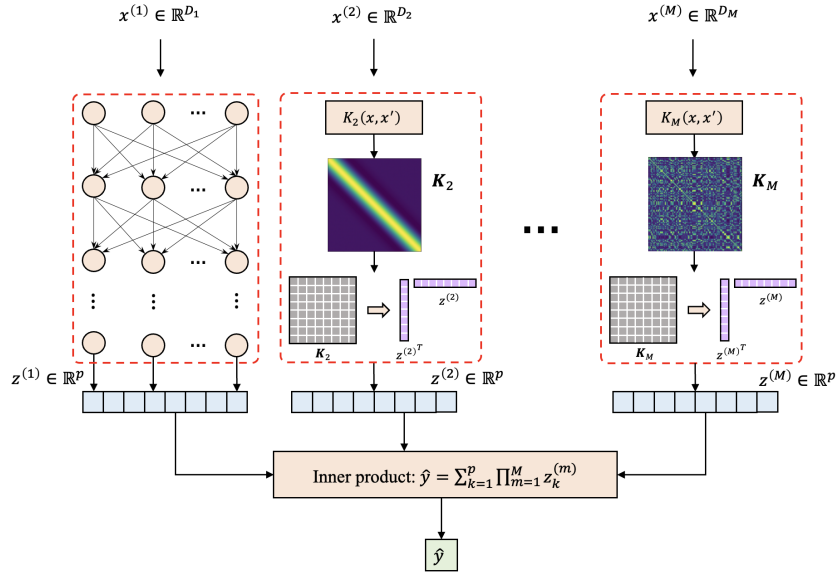


Figure A2: Given data containing  $M$  sources of information  $\mathbf{x} = \{x^{(1)}, x^{(2)}, \dots, x^{(M)}\}$ , we can process the data using our ICK framework where high-dimensional information (e.g.  $x^{(1)}$  in the figure) is processed using a neural network and low-dimensional information (e.g.  $x^{(2)}$  in the figure) is processed using a kernel function followed by Nyström or RFF transformation.

## A ICK with More Than Two Kernels

Besides the visualization presented in Figure 1, we also show our ICK framework for processing data  $\mathbf{x} = \{x^{(1)}, x^{(2)}, \dots, x^{(M)}\}$  with  $M > 2$  sources of information in Figure A2. Here  $K^{(2)}, \dots, K^{(M)}$  represent different types of kernels with trainable parameters. The final prediction is calculated by a chained inner product of all extracted representations  $\hat{y} = \sum_{k=1}^p \prod_{m=1}^M z_k^{(m)}$ .

To confirm that ICKy can work with more than 2 kernels, we construct another synthetic data set containing 3000 data points in total. Each input  $\mathbf{x} = \{x^{(1)}, x^{(2)}, x^{(3)}\}$  has 3 sources of information. The output  $y$  is generated by  $y = x^{(3)} \tanh(2x^{(1)} \cos^2(\pi x^{(2)}/50)) + \epsilon$  where  $\epsilon$  is a Gaussian noise term. We process  $x^{(1)}$  with a small single-hidden-layer NN,  $x^{(2)}$  with an *exponential sine squared* kernel, and  $x^{(3)}$  with a *radial-basis function* (RBF) kernel. Figure A1 shows the prediction results as we progressively add more sources of information into our ICKy framework with corresponding kernel functions. It can be observed that ICKy yields both smallest error and highest correlation

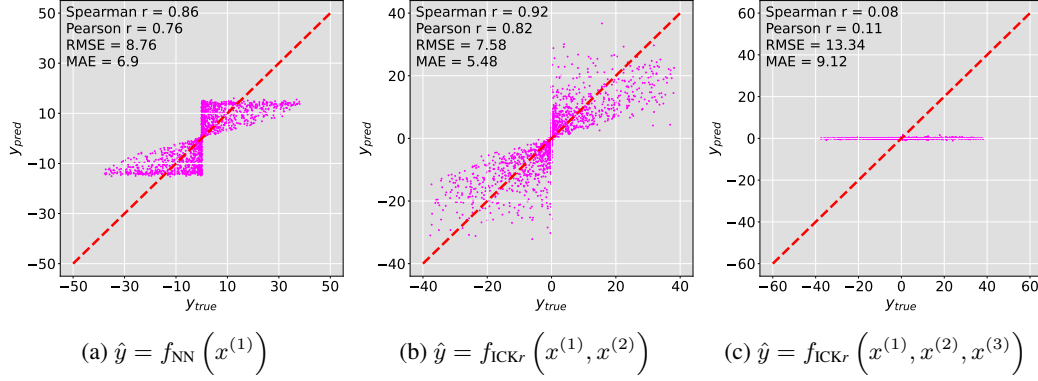


Figure B1: Scatter plots of the true values of  $y$  against the predicted values of  $y$  using our ICKr framework with (a) one source of information, (b) 2 sources of information, and (c) 3 sources of information. Note that here we use RFF for kernel-to-latent-space transformation.

with information from all 3 different sources. Hence, ICKy works well with the  $M = 3$  case and the regression performance is improved as we add in more information related to the target.

## B Random Fourier Features

### B.1 Methodology

Random Fourier Features (RFF) is another popular approximation method used for kernel learning [34]. Unlike the Nyström method which approximates the entire kernel matrix, RFF directly approximates the kernel function  $K$  using some randomized feature mapping  $\phi: \mathbb{R}^{D_m} \rightarrow \mathbb{R}^{2d_m}$  such that  $K(x_i^{(m)}, x_j^{(m)}) \approx \phi(x_i^{(m)})^T \phi(x_j^{(m)})$ . To obtain the feature mapping  $\phi$ , based on Bochner's theorem, we first compute the Fourier transform  $p$  of kernel  $K$

$$p(\omega) = \frac{1}{(2\pi)^{D_m}} \int_{-\infty}^{+\infty} e^{-j\omega^T \delta} K(\delta) d\delta, \quad (14)$$

where  $\delta = x_i^{(m)} - x_j^{(m)}$ . Then we draw  $d_m$  i.i.d. samples  $\omega_1, \omega_2, \dots, \omega_{d_m}$  from  $p(\omega)$  and construct the feature mapping  $\phi$  as follows

$$\phi(x^{(m)}) \equiv d_m^{-1/2} \left[ \cos(\omega_1^T x^{(m)}), \dots, \cos(\omega_{d_m}^T x^{(m)}), \sin(\omega_1^T x^{(m)}), \dots, \sin(\omega_{d_m}^T x^{(m)}) \right]. \quad (15)$$

Since  $\phi(x^{(m)}) \in \mathbb{R}^{2d_m}$ , we need to set  $d_m = p/2$  when using RFF as a kernel-to-latent-space transformation. In addition, since RFF involves sampling from a distribution, the kernel parameters are thus not directly differentiable and we need to apply a reparameterization trick [25] to learn those parameters.

### B.2 Experimental Results

#### B.2.1 Synthetic Data

We use the same toy data set where each data point  $x = \{x^{(1)}, x^{(2)}, x^{(3)}\}$  contains 3 sources of information as described in Appendix A. Also, we use the same types of kernels as those in ICKy as discussed in Appendix A. The only difference here is that we use RFF instead of Nyström method to transform the kernel matrix into the latent space in ICKr framework.

The results are displayed in Figure B1. It can be observed that when we add in only the side information  $x^{(2)}$  along with the *exponential sine squared* kernel, both the correlation and the predictive performance are improved (though not as good as the results from ICKy as shown in Figure A1).

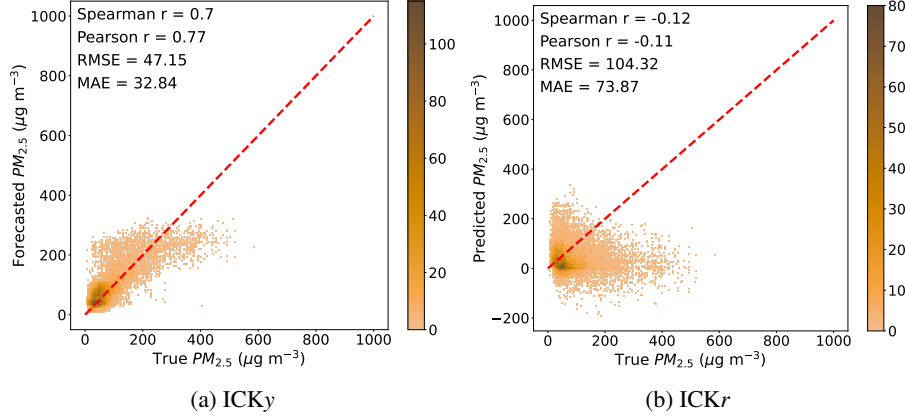


Figure B2: Density plots of the true  $PM_{2.5}$  concentrations against the forecasted  $PM_{2.5}$  concentrations for  $t \geq 500$  using our ICK framework with (a) ICKy and (b) ICKr

However, after we further include  $x^{(3)}$  with the *RBF* kernel, we realize that the parameters of ICKr become very hard to optimize and it fails to make valid predictions and starts to guess randomly around zero.

### B.2.2 Remote Sensing Data

We also try ICKr on the *forecasting* task using the remote sensing data (see Section 5.2) and compare the results with those from ICKy. Each data point  $x = \{x, t\}$  contains a satellite image  $x$  as the high-dimensional information and its corresponding timestamp  $t$  as the low-dimensional information. The satellite images are processed with a two-layer CNN and the timestamps are processed with an *exponential-sine-squared* kernel with a period of  $T = 365$  (days). As can be observed from Figure B2, ICKr yields much higher error compared to ICKy.

## C Eigen-spectrum of the Kernel Matrix

Yang et al. [44] studied the fundamental difference between Nyström method and Random Fourier Features (RFF). They conclude that Nyström-method-based approaches can yield much better generalization error bound than RFF-based approaches if there exists a large gap in the eigen-spectrum of the kernel matrix. This phenomenon is mainly caused by how these two methods construct their basis functions. In particular, the basis functions used by RFF are sampled from a Gaussian distribution that is independent from the training examples, while the basis functions used by the Nyström method are sampled from the training samples so they are data-dependent. In our synthetic data experiments, we train our ICK framework using a batch size of 50. The eigenvalues of the kernel matrices computed from the first 4 batches of the synthetic data set are displayed in Figure C1. It can be observed that the first few eigenvalues of the kernel matrix are much larger than the remaining eigenvalues. Namely, there exists a large gap in the eigen-spectrum of the kernel matrix, which helps explain why ICKy has a much better performance than ICKr.

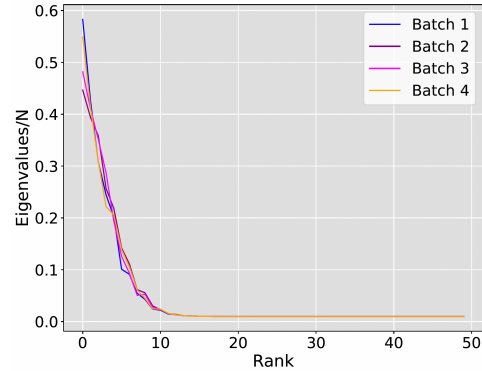


Figure C1: Eigenvalues of the kernel matrix computed from the first 4 batches of training data

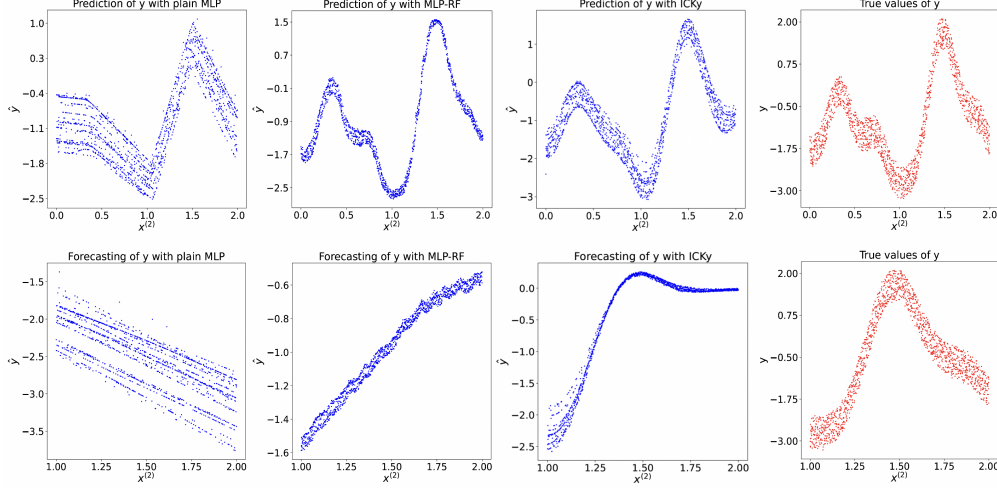


Figure D1: Prediction (top row) and forecasting (bottom row) of  $y \sim \mathcal{GP}(0, K_1 + K_2)$ , where  $x^{(1)}$  is input to a linear kernel  $K_1$  and  $x^{(2)}$  is input to a spectral mixture kernel  $K_2$ . Here we only plot  $x^{(2)}$  against the predicted  $y$ . We implement 3 types of models: plain MLP (left column), MLP-RF (middle left column), and our ICKy framework (middle right column), and we compare the results with the true values of  $y$  (right column).

## D Simulation of an Additive Kernel

While ICK is designed to capture multiplicative kernels, we evaluated how well it could capture additive kernels. We conduct experiments using another synthetic data set generated by an additive kernel  $y \sim \mathcal{GP}(0, K_1 + K_2)$  with the same training settings. As shown in Figure D1, ICKy again outperforms plain MLP and MLP-RF in both the prediction and the forecasting tasks. Moreover, we again test plain MLP, MLP-RF, and ICKy on the prediction task using different number of training samples. As displayed in Figure D2, ICKy yields the smallest error among all the 3 frameworks. Also, the performance gap between ICKy and the other 2 benchmark models shrink as we feed in more training data. Therefore, we conclude ICKy is robust enough to simulate both additive and multiplicative kernels.

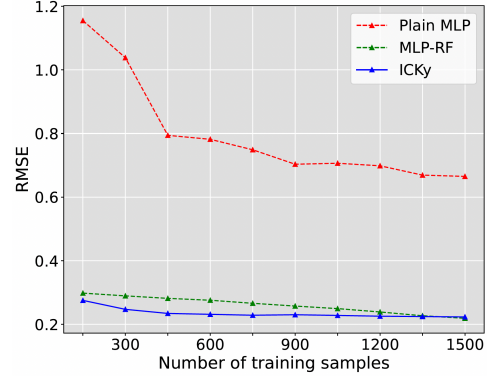


Figure D2: Prediction error of plain MLP, MLP-RF, and ICKy with different amount of training data generated by  $y \sim \mathcal{GP}(0, K_1 + K_2)$



## E Number of Integrating Points

As discussed in Section 4.2.1, as we increase the number of integrating points  $p$ , we expect the approximation error between the true kernel matrix  $\mathbf{K}$  and the approximated kernel matrix  $\hat{\mathbf{K}}$  to decrease. Here, we do empirically show how the value of  $p$  impacts our predictions. In Figure E1, we plot the prediction error of  $\hat{y} = f_{\text{ICKy}}(x^{(1)}, x^{(2)}, x^{(3)})$  against the number of integrating points using the synthetic data generated in Appendix A. As can be observed, the prediction error drops sharply as we raise  $p$  from a small value (e.g.  $p = 2$ ). When  $p$  is relatively large, increasing  $p$  yields smaller improvement on the predictions. Since updating the Cholesky decomposition scales  $\mathcal{O}(p^3)$ , there is a tradeoff between performance and computational complexity, which we believe is an important factor to consider when choosing the value of  $p$ .

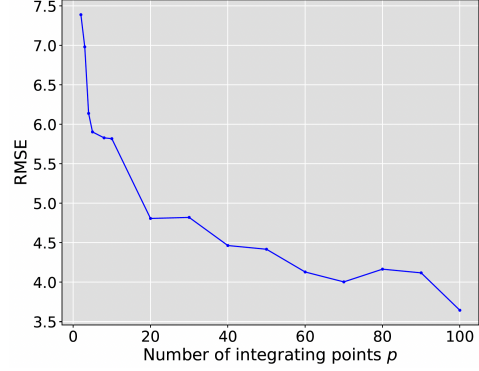


Figure E1: Plot of prediction error of  $\hat{y} = f_{\text{ICKy}}(x^{(1)}, x^{(2)}, x^{(3)})$  against the number of integrating points  $p$

## F Visualization of Remote Sensing Data as Time Series

To better illustrate the results in Section 5.2, we visualize those results in the form of time series. As shown in Figure F1, the plain CNN-RF model does not work as it tends to forecast constant  $\text{PM}_{2.5}$  values. In contrast, both the seasonal CNN-RF model and our ICKy framework captures the overall trend of the true daily averaged  $\text{PM}_{2.5}$  values, but the forecasted values by ICKy are smoother and yield smaller error.

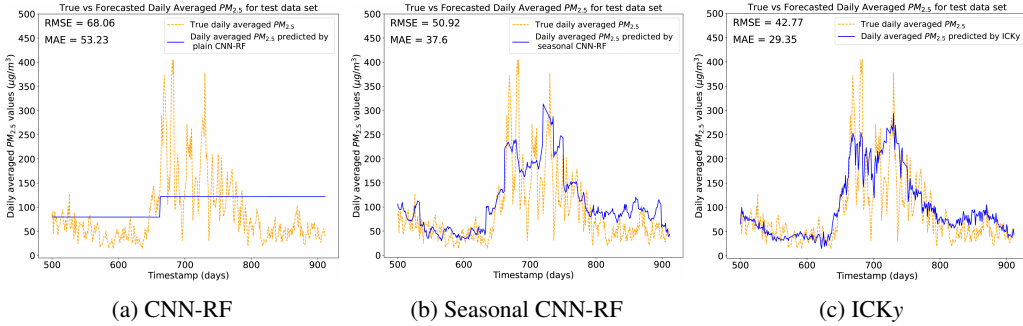


Figure F1: Time series visualization of the true against the forecasted *daily averaged*  $\text{PM}_{2.5}$  concentrations for  $t \geq 500$  using (a) a CNN-RF joint model [46, 47], (b) a CNN-RF joint model with seasonality incorporated, and (c) our ICKy framework

## G Generation, Accessibility, and Restrictions of the Data

The synthetic data  $y \sim \mathcal{GP}(0, K_1 K_2)$  in Section 5.1 and  $y \sim \mathcal{GP}(0, K_1 + K_2)$  in Appendix D are generated using the GPyTorch package. The remote sensing data in Section 5.2 is downloaded using PlanetScope API whose content is protected by copyright and/or other intellectual property laws. To access the data on PlanetScope, the purchase of an end-user license is required. When this manuscript is accepted, we will provide the codes we used to acquire the data. The UCI machine learning repository data we use in Section 5.3 has an open access license, meaning that the data is freely available online.